JOURNAL OF MECHANICAL ENGINEERING AND SCIENCES (JMES)
ISSN: 2289-4659 e-ISSN: 2231-8380
VOL. 16, ISSUE 1, 8718 – 8729
DOI: https://doi.org/10.15282/jmes.16.1.2022.06.0689

UNIVERSITI MALAYSIA PAHANG

ORIGINAL ARTICLE

Mechanics of solder/IMC interface of lead-free solder interconnects in ball grid array assembly

S. F. M. Asasaari, N. A. Fadil, M. N. Tamin*

School of Mechanical Engineering, Faculty of Engineering, Universiti Teknologi Malaysia, 81310 Johor Bahru, Malaysia.
*Phone: +60127781410; Fax: +6075566159

ABSTRACT – The lead-free Sn-0.4Ag-0.5Cu (SAC405) solder arrays provides an interconnection between the electronic package and printed circuit board (PCB) of the assembly. The ball grid array (BGA) test assembly was exposed to thermo-mechanical loading during solder reflow cooling and subsequent reliability temperature cycles. This could contribute to the solder/IMC interface damage and cracking. Finite element (FE) analysis was utilized to model the BGA assembly under the prescribed temperature loading profile. The unified constitutive (Anand) model was used to describe the temperature- and strain rate-dependent response, and solder/IMC interface damage of the SAC405 solder interconnects. Solder reflow cooling begins from the assumed stress-free reflow temperature of 220 °C to 25 °C at 1.3 °C/s. This was followed by temperature cycling between 125 and -40 °C with 15 minutes dwell time at upper and lower peak temperature levels. The temperature ramp rate of 11 °C/min was used. Results show that the most critically stressed solder joint was the one located underneath the edge of the silicon die. The solder/IMC interface crack initiated at the interface near the package side of the assembly. Catastrophic fracture of the BGA assembly was predicted during the first temperature cycle due to the relatively low input strength and toughness of the brittle-like solder/IMC interface properties. The solder/IMC failure prediction could not be inferred solely from inelastic strain in the bulk solder joint but should also consider the damage of the interface. This study shall benefit the newly designed BGA packages through rapid generation of reliability data and by providing insight into the reliability aspects of the BGA assembly with interface fracture issues.

ARTICLE HISTORY
Received: 12th Aug. 2021
Revised: 29th Sept. 2021
Accepted: 04th Oct. 2021

KEYWORDS
Ball grid array; solder/IMC interface; SAC405 solders; reflow cooling; temperature cycle

INTRODUCTION

Semiconductor technology and electronic packaging are growing rapidly. Consequently, ball grid array (BGA) assembly is becoming important in the electronics industry due to its higher density interconnects and relatively inexpensive [1, 2]. Lead-free solder interconnects using BGA solder joints are essential in microelectronics packaging in meeting customer's demands [2, 3]. The new generation of lead-free solders is designed to suit applications in harsh environments. Therefore, they need to have excellent resistance to withstand the repeated temperature loading and long dwell time at peak temperature. During fabrication and operations, the solder joints are subjected to various types of loading such as reflow temperature [4, 5], temperature cycle [6-9], and drop impact [10-12] that cause both thermal and mechanical stresses.

Lead-free solder interconnects are widely used in microelectronics packages, complying with RoHS directive [13]. Variations of lead-free solder alloys use include Sn-Ag, Sn-Cu, Sn-Ag-Cu, and Sn-Ag-Cu-X with X being the doping elements such as Bi, In, and Zn. The Sn-4Ag-0.5Cu (SAC405) solder alloy is commonly used for reflow and wave soldering. The solder has been considered by authors' research team in the development of reliability models of BGA packages. Consequently, the SAC405 solder interconnects are used in this work as a demonstrator material. The reflowed BGA solder joints with a spherical geometry of 0.45 mm in diameter were assembled on the substrate with electroless nickel immersion gold (ENIG) surface finishes from the industry. Previous works have reported that too thick an intermetallic compound (IMC) at the solder/copper pad interface generates voids and micro-cracks which degrades the reliability of solder interconnects [14-17]. They have investigated the SAC lead-free solder alloys with the compositions ranging from Sn-(2.0-4.0 wt. % Ag)-(0.5-1.0 wt. % Cu). In the critical solder joint, damage occurs progressively over the temperature cycles. A complete fracture is contributed by crack initiation and subsequent propagation of the cracks. In addition, high straining rates loading [18] may cause brittle interface fracture near the solder/IMC or across the IMC layer [12, 19-21]. The slow straining rates may damage the solder joints and result in ductile failure across the bulk solder joint [22]. Therefore, the reliability of solder interconnects becomes a major interest, as they are the weakest link in solder interconnects.

Reliability prediction of solder interconnects from experiments involving temperature cycling and impact loading is relatively expensive and time-consuming. Consequently, a predictive assessment that imitates the actual performance of the BGA assembly is essential. In this respect, this paper quantifies the deformation behavior and fracture of the solder interconnects in BGA assembly using the finite element (FE) method. The FE model of BGA assembly is used to examine

*CORRESPONDING AUTHOR | M. N. Tamin | ✉ nasirtamin@utm.my

© The Authors 2022. Published by Penerbit UMP. This is an open access article under the CC BY license.

and quantify the damage mechanics-based process in the assemblies under reflow cooled down and temperature cycles [23-27]. The effectiveness of FE simulation in predicting the initiation of crack and its propagation in lead-free solder interconnects is influenced by the geometrical model, prescribed boundary conditions and loadings, and the validity of unified constitutive equations. The unified constitutive Anand model adequately describes the temperature- and inelastic strain rate-dependent behavior of the SAC405 solder joints [28]. However, this constitutive model only calculates the hardening or softening behavior of the solder alloy but without predicting the occurrence of fracture.

Fracture of the solder/IMC interface occurred close to the package and/or PCB sides [25, 29]. The brittle interface between the tin-based solder alloy and the IMC layer dictates the reliability of the BGA solder joints [21, 26, 27, 30]. The reliability temperature cycles expose the multi-materials assembly to effects of coefficient of thermal expansion (CTE) mismatches, resulting in cyclic stresses and strain hysteresis. The relatively large strain and stress cycles at the solder/IMC interface have resulted in fatigue crack initiation, and subsequent propagation to catastrophic fracture of the solder interconnects [24, 31]. Such interface cracking processes have been investigated within the fracture mechanics domain [24, 27, 32] and damage mechanics approach [33, 34].

This paper quantifies the mechanics of deformation as well as the interface damage process in the solder/IMC interface of BGA assembly using FE simulation. The temperature starts from the reflowed solder cooled down to room temperature before temperature cycles loading take place. Temperature- and strain rate-dependent properties of the Sn-4Ag-0.5Cu (SAC405) solder alloy and solder/IMC interface strengths are considered. A quadratic stress-based approach is used to define the interface damage initiation.

FINITE ELEMENT MODELING

Geometry of BGA Assembly, Prescribed Boundary Conditions and Loadings

The BGA assembly is modeled with silicon die (package), FR-4 substrate layer, copper pad, Cu_6Sn_5 IMC, and FR-4 PCB. The square ball grid array consists of 100 SAC405 solder interconnects. The solder ball has a diameter of 0.48 mm, a pitch distance of 0.80 mm, and a stand-off height of 0.30 mm. The solder-mask-defined (SMD) edge is modeled at the substrate side, while the non-solder-mask-defined (NSMD) is modeled at the board side, as illustrated in Figure 1. The 2 µm layer of Cu_6Sn_5 IMC between the copper pad and the solder ball is assumed to have formed at the beginning of the reflow process. It is expected that the IMC layer does not grow thicker during the subsequent temperature cycles. The laminated FR-4 substrate layer and the circuit board are modeled as a homogeneous orthotropic material.

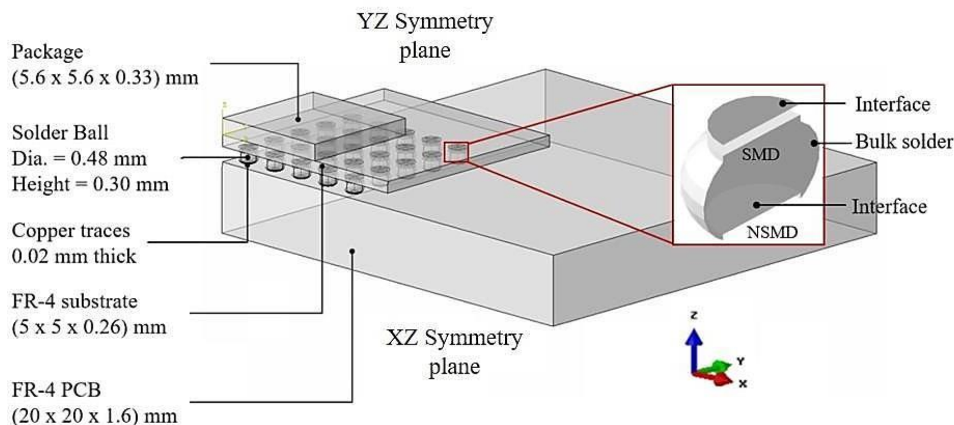

Figure 1. The one-fourth FE model of BGA assembly including component dimensions. The inset figure displays the cut-out geometry of the solder joint with SMD at the package side and NSMD at the board side

While the solder/IMC interfaces are allowed to separate (fracture), other contact surfaces in the model are assumed to be perfectly bonded throughout the temperature loading. One-fourth model of BGA assembly is considered for reliability assessment due to the symmetry of the geometry, loadings, and boundary conditions in symmetric planes, as illustrated in Figure 1. The displacement and rotation at the XZ- and YZ-planes are set to zero, $UR_x = UR_z = U_y = 0$ and $UR_y = UR_z = U_x = 0$, respectively. The coordinate origin (at the assembly's center) is fixed in all the displacement axes to avoid rigid body movement. The solder/IMC interfaces at both package (top) and PCB (bottom) sides are modeled using "zero-thickness" cohesive elements (Abaqus COH3D8 elements) [33, 35]. Such elements would provide the normal and shear stress components of the interface. Other components are discretized using solid elements (Abaqus C3D8R elements).

A series of preliminary runs with successively smaller element sizes are performed for the mesh convergence analysis. The largest element size, without affecting the FE-calculated variables for the critical solder is 0.015 mm. The preliminary runs also identified the critical solder joint located underneath the die edge (solder location D4) to be the most critically stressed during the solder reflow cooling, as illustrated in Figure 2(a). All the solder joints are discretized using the same element mesh in view of the possibility that the solder/IMC interface damage could occur for different solder interconnects. Each solder joint is discretized into 902 solid elements and 1184 nodes (Figure 2(b)). The whole model

consists of 68076 8-node solid elements and 2952 8-node cohesive elements with matching nodes across the solder/IMC interface.

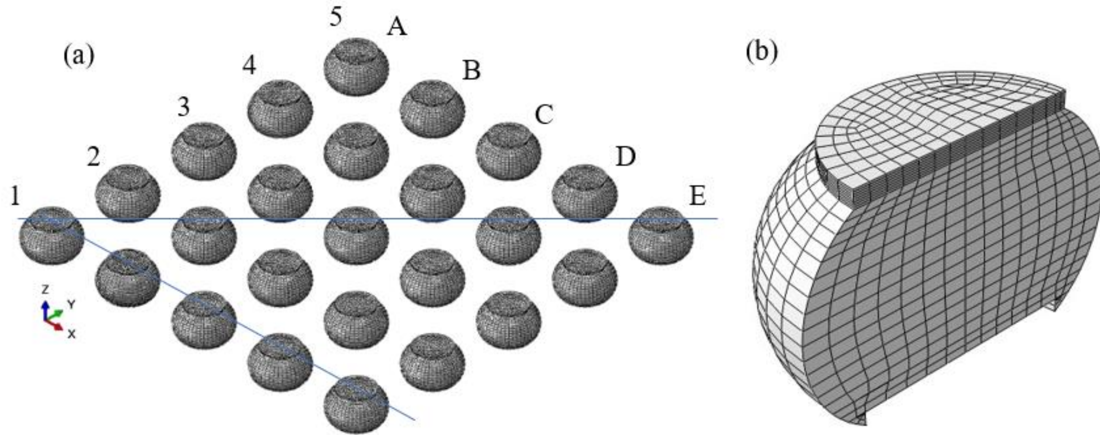

Figure 2. Quarter symmetry of BGA of solder joints showing (a) converged element mesh and (b) Detailed mesh of a solder joint (cut-out section)

Loading

The temperature loading profile, shown in Figure 3, consists of solder reflow cooling (line O-A) from the assumed stress-free reflow temperature of 220 °C for SAC405 solder alloy to ambient temperature (25 °C). The cooling rate is 1.3 °C/s [36, 37]. The subsequent temperature cycle is represented by line (A-B-C-D-E-F-G) for the first cycle. A total of three temperature cycles are simulated. The temperature ranges from 125 °C to -40 °C for the suggested reliability temperature profile with a temperature range of 165 °C [38]. The solder joints are heated and cooled at a rate of 11 °C/min with a 15 minute dwell time at both upper and lower peak temperature levels [38]. The transient heat transfer effect is negligible at these heating and cooling rates [39].

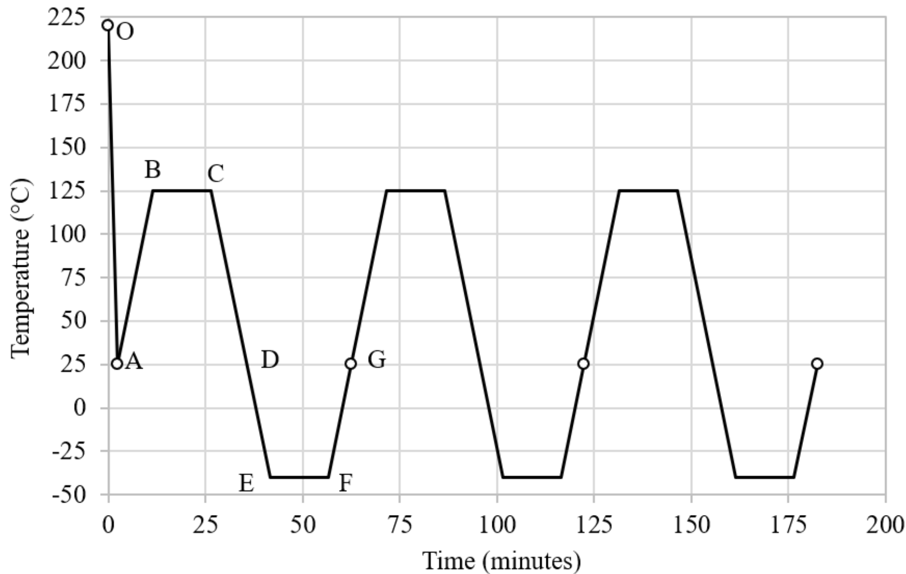

Figure 3. Temperature profile consisting of solder reflow cooling and temperature cycles with dwell-time

Constitutive Model of Solder Alloy and Damage Criterion of Solder/IMC Interface

The unified inelastic strain Anand model [28] with refined model parameters [37] is used to describe the inelastic behavior of lead-free SAC405 solder alloy. The inelastic strain rate, $\dot{\varepsilon}_{in}$ is expressed in terms of the current stress, σ and an evolving internal state variable, s as:

$$\dot{\varepsilon}_{in} = A\, exp\left(-\frac{Q}{RT}\right)\left[sinh\left(\xi\frac{\sigma}{s}\right)\right]^{\frac{1}{m}} \tag{1}$$

where A is the pre-exponential factor, Q is the activation energy, R is the gas constant (Boltzmann's constant), m is the strain rate sensitivity, and ξ denotes the stress multiplier. The temperature, T measured in Kelvin scale. The internal state variable, s evolves as follows:

$$\dot{s} = \left\{h_0 \left|1 - \frac{s}{s^*}\right|^a . sgn\left(1 - \frac{s}{s^*}\right)\right\} . \dot{\varepsilon}_{in} \tag{2}$$

where a is the strain rate sensitivity of the hardening parameter. The sign function is defined as:

$$sgn(x) = \begin{cases} 1, & x \geq 0 \\ -1, & x < 0 \end{cases} \tag{3}$$

Both the initial value of the internal state variable, s_0, and hardening parameter, h_0, are further expressed as temperature- and strain rate-dependent quantities, as provided in Eqs. (5) and (6), respectively [37]. The coefficients in these equations were computed using previously published empirical data for SAC405 solders performed at various test temperatures ranging from 25 °C to 150 °C and different strain rates varying from 10^{-5} s^{-1} to 10^{-3} s^{-1} [40]. The stress saturation rate, s^* is calculated as follows:

$$s^* = \hat{s} \left[\frac{\dot{\varepsilon}_{in}}{A} exp\left(\frac{Q}{RT}\right)\right]^n \tag{4}$$

where n is the strain rate sensitivity of the saturation value, $\hat{s}$ is a deformation resistance saturation value.

The flow Eq. (1) accounts for the creep and viscoplastic behavior of the solder alloy. This unified inelastic strain constitutive model does not require any explicit yield criterion, thus could be used without regard to the direction of the loading. Table 1 shows the model parameters for SAC405 solder alloy.

Table 1. Parameters for unified constitutive Anand model of SAC405 solders [37]

Anand Parameters	A (s^{-1})	Q/R (K)	m	n	$\hat{s}$ (MPa)	ξ	a	s_0 (MPa)	h_0 (MPa)
Value	7128	10561	0.8181	1.091 x 10^{-3}	30.45	10	1.6	Eq. (5)	Eq. (6)

$$s_0 = 25.996 - 1.4772 \times 10^{-2} T + 7.386 \times 10^{-6} T^2 \tag{5}$$

$$h_0 = 9.85 \times 10^4 - 880\, T + 2.2\, T^2 - 2.1 \times 10^6\, \dot{\varepsilon}_{in} + 1.05 \times 10^8\, \dot{\varepsilon}_{in}^2 \tag{6}$$

Figure 4 illustrates the predictive performance of the material model for SAC405 solder alloy at selected test temperature levels and strain rates. A good correlation between the predicted and measured stress-strain curves of the material is demonstrated. Thus, the unified inelastic Anand constitutive model is employed for the solder alloy in the FE simulations of the BGA package.

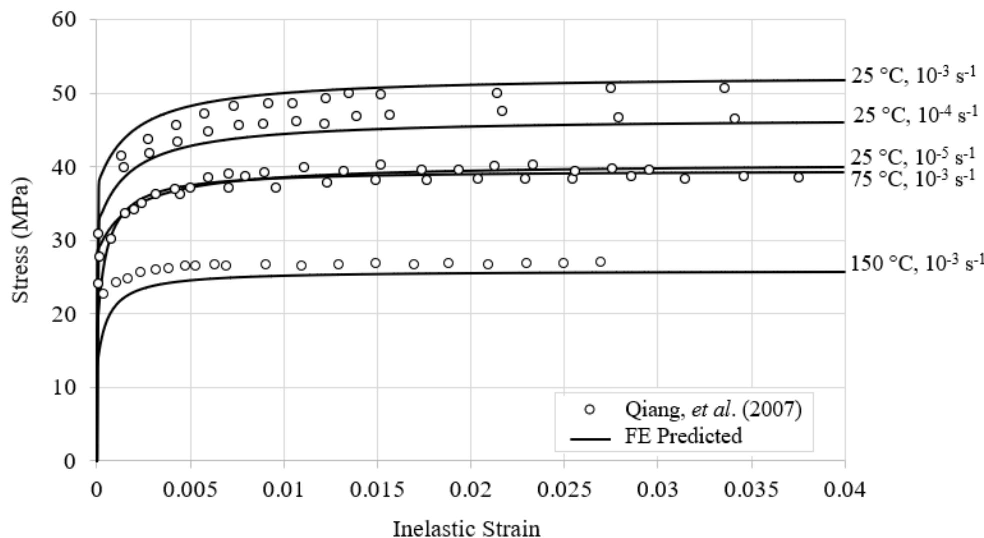

Figure 4. The stress-inelastic strain curves of SAC405 solder joints at varying straining rates and temperature levels. Data points are extracted from [40]

Other materials are assumed to behave elastically with temperature-dependent properties over the prescribed temperature range. In addition, the orthotropic behavior of FR-4 substrate and PCB is considered. Table 2 provides the relevant material properties used in the simulation.

Table 2. Materials properties used in the FE model [40-44]

Material	Young's modulus (GPa)	Poisson's ratio, v	CTE, α (ppm/°C)
Sn4.0Ag0.5Cu	44.7 – 0.146 T	0.36	20
Si-die	132.46 – 0.00954 T	0.28	2.113 + 0.00235 T
Copper layer	141.92 – 0.0442 T	0.35	15.64 + 0.0041 T
Cu_6Sn_5	85.6	0.31	16

FR-4 PCB & Substrate (isotropic in xy-plane)			
Shear modulus, G (GPa)	Young's modulus, E (GPa)	Poisson's ratio, v	CTE, α (ppm/°C)
12.60 – 0.0167 T (G_{xy})	27.92 – 0.0370 T (E_x, E_y)	0.11(v_{xy})	16 (α_x, α_y)
5.50 – 0.0073 T (G_{xz}, G_{yz})	12.60 – 0.0167 T (E_z)	0.39 (v_{yz}, v_{xz})	84 (α_z)

*T is temperature in Kelvin scale

The material properties of the solder/IMC interface were determined through a combined experimental-computational approach [45]. Solder ball shear push tests and solder ball pull tests were performed using a Dage 4000 bond tester. The measured load-displacement curve to fracture of each solder joint is established. Complimentary FE modeling of the experiment is performed to match the measured stiffness while the calculated local stress at fracture is taken to correspond to the strength of the interface for the observed interface fracture. The effects of temperature and strain rate on the SAC405 solder/IMC interface strength are summarized in Figure 5. The interface normal (tensile) strength, N and shear strength, S can be expressed as:

$$N(T, \dot{\varepsilon}) = -6.4\, ln(T) - 9.1\, ln(\dot{\varepsilon}) - 2.8 \tag{7}$$

$$S(T, \dot{\varepsilon}) = -1.8\, ln(T) - 4.5\, ln(\dot{\varepsilon}) - 10.2 \tag{8}$$

The strain rate-dependent strength properties of the interface are likely derived from the rate-dependency of the adjacent bulk solder alloy. In addition, the decreasing trend of the strength properties of the solder/IMC interface with increasing strain rates has been reported [21, 46]. Other parameter values, such as the penalty stiffness and the critical energy release rates (G_{IC} and G_{IIC}) in normal and shear loading are scaled appropriately with a similar trend. The respective values are listed in Table 3.

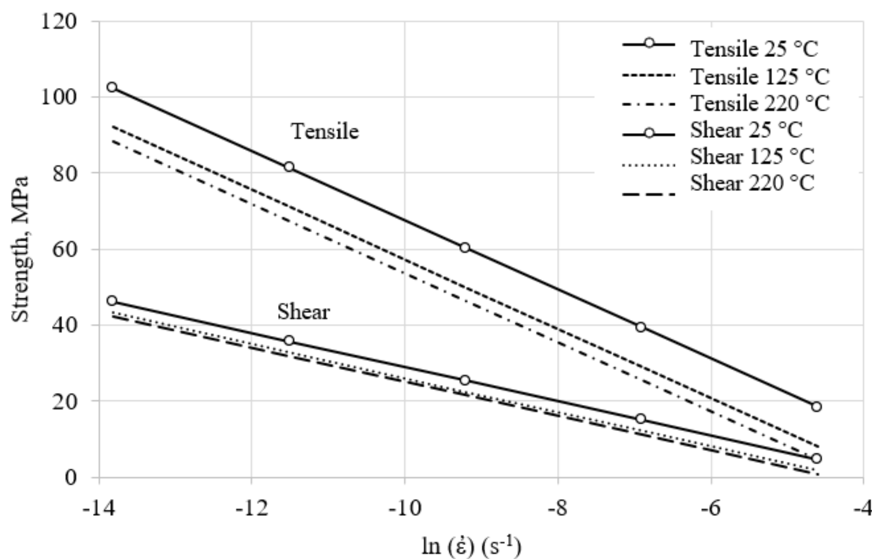

Figure 5. SAC405 solder/IMC interface strengths as functions of strain rates and temperatures

Table 3. Temperature-dependent properties of solder/IMC interface

Parameters \ Temperature (°C)	25	75	150	220
Tensile stiffness, k_n (MPa)	16400	11960	9186.4	5864.4
Shear stiffness, k_s (MPa)	6000	5014.4	4542.8	3792.8
Normal strength, N (MPa)	22.7	16.6	12.7	8.1
Shear strength, S (MPa)	11.2	9.1	7.9	7.1
Critical energy release rate for Mode I, G_{IC} (N/mm)	0.0196	0.0116	0.0088	0.0056
Critical energy release rate for Mode II, G_{IIC} (N/mm)	0.0168	0.0140	0.0128	0.0108

The solder/IMC interface fracture process involves a damage initiation event and subsequent damage evolution up to the separation (fracture) of the interface material point. The cohesive behavior of the brittle-like interface is modeled using the bilinear traction-displacement softening law. The onset of damage, as dictated by the stress-based criterion for the tension-shear loading of the interface, is expressed as [47]:

$$\sqrt{\left(\frac{\langle\sigma_{33}\rangle}{N(T,\dot{\varepsilon})}\right)^2+\left(\frac{\tau_{13}}{S(T,\dot{\varepsilon})}\right)^2+\left(\frac{\tau_{23}}{S(T,\dot{\varepsilon})}\right)^2}=1 \quad (9)$$

where $\langle\sigma_{33}\rangle$ is the tensile normal, τ_{13} and τ_{23} are the shear traction components on the solder/IMC interface plane. The Macaulay bracket, <·> indicates that the compressive stress does not contribute to the damage.

Following the damage initiation event, the degradation of the penalty stiffness of the solder/IMC interface is expressed in terms of the energy release rates, $G_T = G_I + G_{II}$ and the single-mode critical values, G_{IC} and G_{IIC} for Mode I and Mode II crack loading, respectively. A linear interaction between the tensile and shear fracture is assumed [39]. The energy-based criterion for fracture (separation) of the interface material point is written as:

$$G_T = G_{IC}(T,\dot{\varepsilon})+\left(G_{IIC}(T,\dot{\varepsilon})-G_{IC}(T,\dot{\varepsilon})\right)\left(\frac{G_{II}}{G_T}\right) \quad (10)$$

RESULTS AND DISCUSSION

The findings of this study are described and interpreted with respect to the deformation and damage process of the BGA assembly during solder reflow cooling and subsequent temperature cycles. The evolution of stresses, inelastic strains, and interface damage of the solder/IMC for the critical solder interconnect in an array are quantified. In this study, the accumulation of separated interface material points is considered as the propagation of interface cracks. The accumulation of interface damage that is dependent on temperature and strain rate is also quantified.

Evolution Characteristics of Solder/IMC Interface Damage

Thermal stresses and strains continuously evolve throughout the cooling of reflowed solder and cycled temperature, owing to the CTE mismatches among the different materials making up the assembly. Two solder interconnects in the array are of particular interest: solder joint D4, which initially exhibits large deformation, and solder joint B1, which experiences severe accumulated damage. Figure 6 shows a comparison of the history plot of the damage initiation variable at the critical point, labeled by A, in both solder/IMC interface planes. Results showed that the damage initiation variable evolves quadratically, as prescribed in Eq. (9). The damage initiation variable reaches unity in solder joint B1 to caused damage initiation at low temperature (32 ºC) following the cool-down stage. It is noted that only a small edge region of the SMD interface at the package side of the assembly is affected. This edge region of the solder joint suffers from geometric discontinuity and severe local CTE mismatches among the metallic solder, copper pad, and IMC layer resulting in local stress gradient [48]. A similar location of solder/IMC interface fracture also has been experimentally observed at the package sides for typical ceramic BGA assembly when subjected to temperature cycles [49].

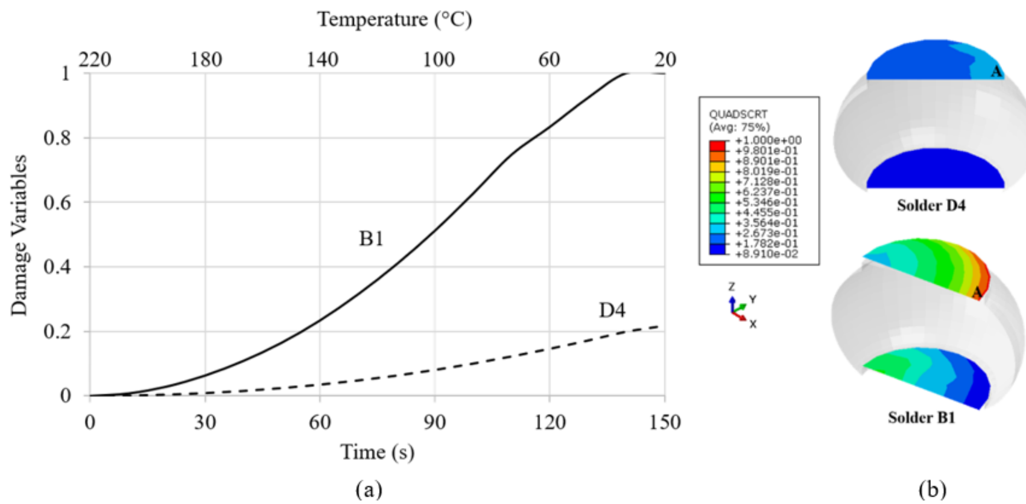

Figure 6. (a) Evolution of the damage initiation variable in the solder/IMC interface for solder D4 and solder B1 during solder reflow cooling process and (b) Distribution of damage variables in the solder/IMC interface at 25 °C

The normal stress distribution in solder interconnects B1 and D4, and the corresponding solder/IMC interface plane at ambient temperature following the solder reflow cooling is compared in Figure 7. Results show that solder joint D4 experiences a large compressive stress gradient across the bulk solder. This also results in flexural stresses in the interface planes. Since the compressive normal stress component does not contribute to interface damage, the computed damage initiation variable magnitude is low (see Figure 6). On the other hand, the SMD interface of interconnect B1 is primarily under tensile stresses that facilitate the onset of damage. At 25 °C, the localized region A has experienced damage initiation and a small drop in stress is indicated.

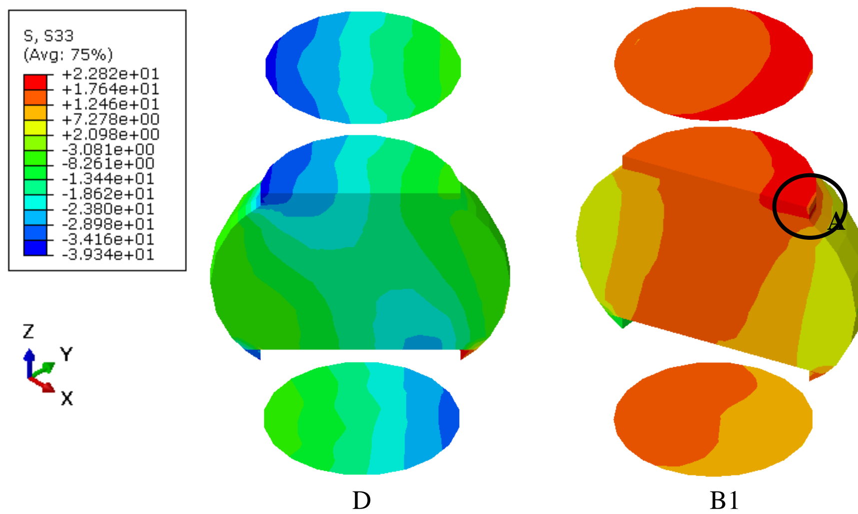

Figure 7. Distribution of normal stress component, σ_z in solder joints D4 and B1, and the corresponding solder/IMC interface plane at 25 °C, at the end of solder reflow cooling

The mechanics of solder/IMC interface damage and fracture process for the critical material point of the interface for solder joint B1 are addressed. The evolution of the damage initiation variable, interface damage, and the normal traction is shown in Figure 8. The evolution of the damage variable during solder reflow cooling (line O-A) has been described using Figure 6. Elastic interface normal traction reaches a level of 22.8 MPa following the reflow cool-down at 25 °C. The corresponding resultant shear traction is 6.7 MPa. Damage has initiated to a magnitude of 0.185 at the edge of the SMD region. Subsequent heating (line A-B) reduces the stress without any contribution to the accumulated damage. The dwell period at 125 °C induces creep strain in the solder near the solder/IMC interface, which negligibly contributes to damage of the interface. The cooling part of the cycle (line C-D-E) increases the stress causing the damage level to reach unity around 36 minutes (at condition D), suggesting separation of the interface material point. This fracture event corresponds to the normal traction of magnitude in the order of the tensile strength of the interface at 25 °C. It is noted that the accumulated damage rises sharply to cause the separation of the interface material point, signifying brittle-like fracture of the solder/IMC interface. Once the material point separates, the traction diminishes, as depicted in Figure 8. The stress previously carried by this point is redistributed among neighboring points through the equilibrium of forces requirements for the next load increment.

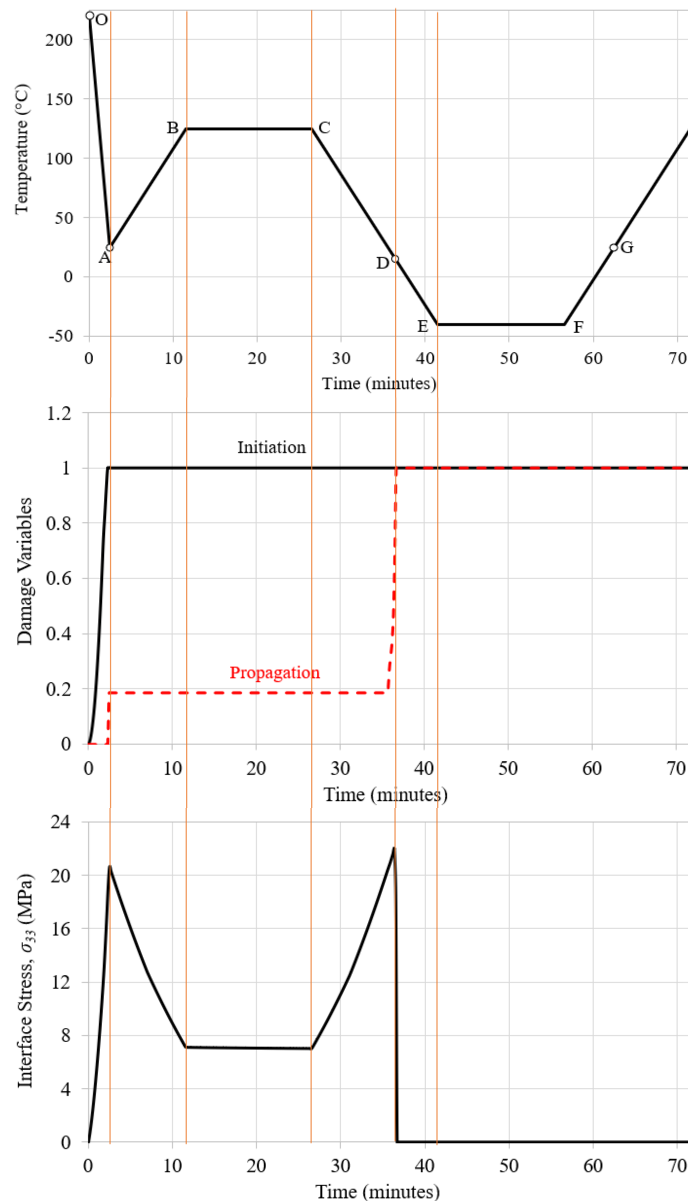

Figure 8. Evolution characteristics of interface damage and normal traction at the critical solder/IMC interface material point for solder joint B1 during solder reflowed cooling and temperature cycles

Solder/IMC Interface Damage Distribution

As shown in Figure 9, the solder/IMC interface damage process is also described using the distribution of the damage initiation variable and subsequent interface damage for the critical solder joint B1. Each figure corresponds to the different sampling times (and temperature levels) throughout the first temperature cycle. The contour at condition A (at 25 °C) following the solder reflow cooling serves as the reference damage condition. As indicated in Figure 8, insignificant damage progresses for the first one-half temperature cycle (line A-B-C-D). In addition, the damage is limited to the edge region of the SMD of the interface, at the package side of the assembly, as illustrated in Figure 9 (bottom row, sampling condition D). A similar fracture location has also been observed experimentally during temperature cycling tests [29]. Further cooling towards -40 °C (line D-E) induced additional stresses, causing damage to have reached the critical value at separation. Complete fracture of the critical solder/IMC interface is predicted. Such early predicted interface fracture of solder joint B1 is likely due to the low prescribed solder/IMC interface properties.

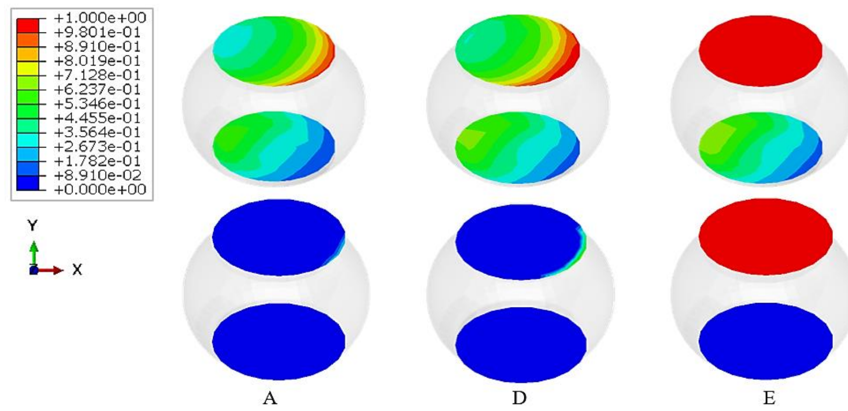

Figure 9. Evolution of damage initiation variable (Top row) and solder/IMC interface damage (bottom row) for the critical solder B1. The time sequence (A, D and E) is as indicated in Figure 8. The threshold value for both damage initiation and separation events are set to 0.98

The spatial distribution of the damage initiation variable and interface damage for the array of the solder interconnects is shown in Figure 10, for selected condition A (reference, 25 °C) and E (-40 °C) during the temperature cycle. Results show that the solder/IMC interface of solder joints located in the middle of the assembly underneath the package (Si-die) are critically stressed. The package side (top) interface plane is experiencing tension resulting from the convex (sad face) configuration of the warpage, thus facilitating the solder/IMC interface damage. Interface separation (or crack initiation) is not predicted at condition A following the solder reflow cooling. At condition E, the assembly has undergone large ΔT of 165 ^{o}C resulting in excessive thermally induced strains and stresses in the solder joints. This has led to solder/IMC interface fracture of 60 % of the solder joints in the array. The predicted failure of the BGA assembly owes to the relatively low solder/IMC interface strength and toughness. Although such premature catastrophic failure is rarely encountered in manufacturing practice, nevertheless it demonstrates the ability of the FE-simulation to capture the fracture mechanism of the brittle-like solder/IMC interface. Improvement in interface properties and solder array geometry could be made and their sensitivity to the reliability of the assembly could be established.

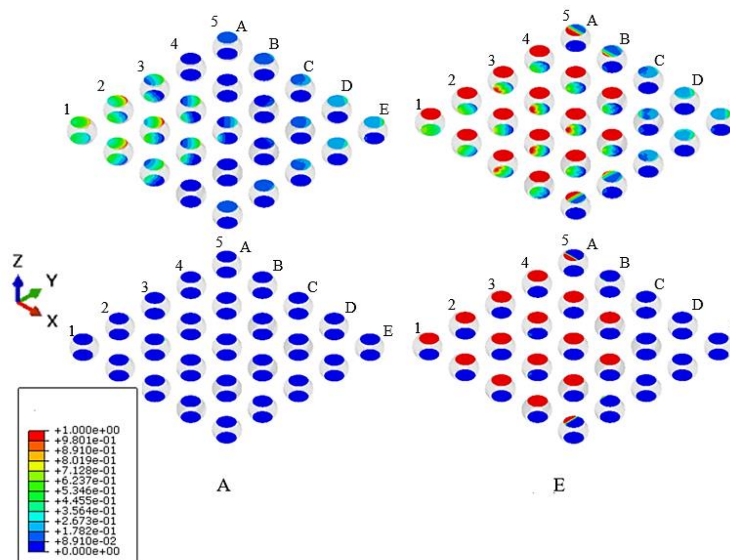

Figure 10. Spatial distribution of damage initiation variable (top row) and solder/IMC interface damage (bottom row) at the selected condition: (a) Condition A (reference, 25 °C) following solder reflow cooling, and (b) Condition E at -40 °C during the first temperature cycle

Inelastic Strain Evolution in SAC405 Solders

Since the adjacent SAC405 solder and Cu_6Sn_5 IMC layer contribute to the stresses and strains of the solder/IMC interface, the evolution of the inelastic strain in the bulk solder, particularly in the region of its interface, should be considered. The characteristic evolution of inelastic strain in selected solder joints throughout the reflow cooling and subsequent temperature cycling is shown in Figure 11. Results show that the solder joint at location D4 accumulated the greatest inelastic strain compared to its adjacent solder joints. Being at the corner of the Si-die (package), this solder joint suffered the largest deflection (warpage), thus, the strain gradient across the interface. The inelastic strain evolves at the rate of 1.82 x 10^{-4} s^{-1} during the solder reflow cooling stage resulting in the local equivalent inelastic strain magnitude of

2.3 % at 25 °C. The strain accumulates to a magnitude of 7.6 % during the first temperature cycle. A negligible amount of additional strain is predicted in subsequent temperature cycles, likely because the solder/IMC interface of the solder joint has fractured. Although the adjacent solder joints accumulate about 50 % less inelastic strain after the first cycle (condition G), these solder joints also experience interface fracture at the solder/IMC. It suggests that the prediction of interface fracture mechanism could not be inferred from inelastic strains in the bulk solder alone but should account for the damage of the solder /IMC interface itself. This is further illustrated by the predicted largest inelastic strain magnitude in solder D4 while solder/IMC interface fracture first occurred in solder B1.

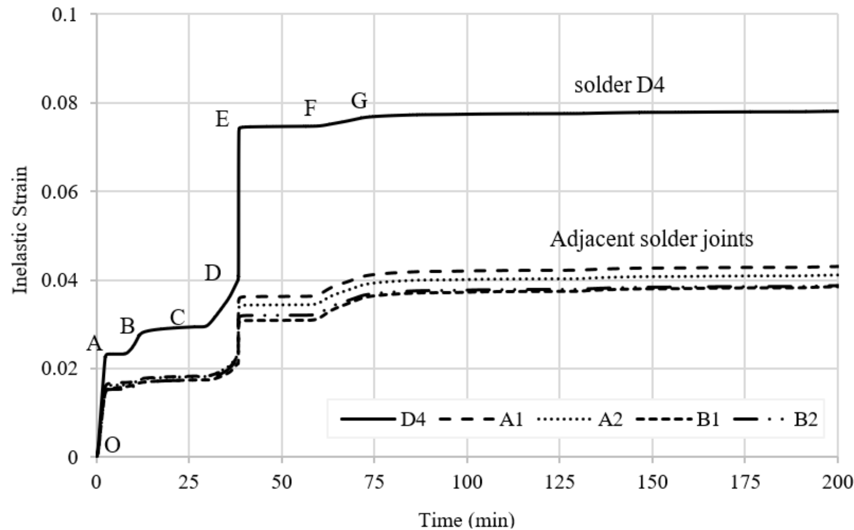

Figure 11. Evolution of inelastic strain at selected solder joints during solder reflow cooling stage (line O-A) and subsequent three temperature cycles

It is noted that the inelastic strain in the critical solder joint is concentrated at the locality next to the NSMD region, at the board side of the assembly, as shown in Figure 12. Although not addressed in this paper, such significant inelastic strain magnitude could initiate fatigue crack in the bulk solder side of the interconnect. Fracture of the bulk solder joint has also been observed for BGA assembly during temperature cycling [22, 50, 51].

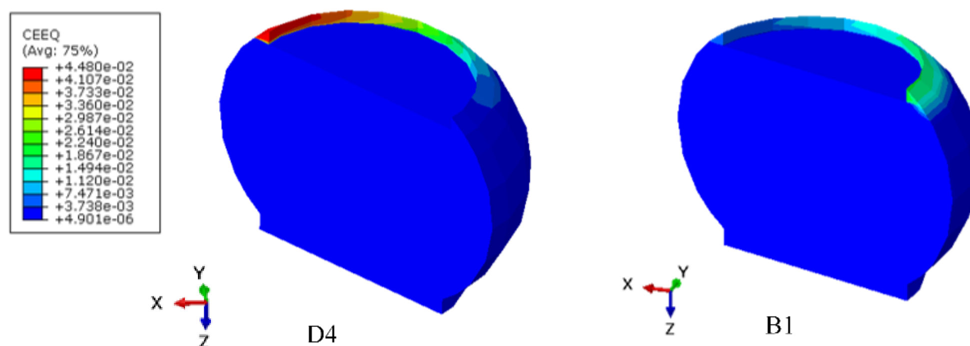

Figure 12. Inelastic strain field in (a) solder joint D4 and (b) solder joint B1 at 25 °C following the solder reflow cooling stage

CONCLUSIONS

Finite element simulation of SAC405 solders in the BGA assembly has been performed using the temperature- and strain rate-dependent behavior of SAC405 solder material and solder/IMC interface throughout solder reflow cooling and temperature cycling. Results showed that:

a) During the solder reflow cooling stage the solder/IMC interface damage initiated at the most critical solder joint, located underneath the corner of the SI-die. However, the interface material point remains intact.

b) Solder/IMC interface fracture is predicted for the interconnect at the package side of the assembly during the first temperature cycle. The corresponding normal and shear traction reaches 22.8 MPa and 6.7 MPa, respectively, at the onset of fracture and diminish immediately.

c) Although the local inelastic strain is largest in the solder joint located at D4, crack initiated first at the solder/IMC interface of solder joint B1. Thus, failure prediction of the interface should not be inferred solely from the inelastic strain of the bulk solder joints but also consider the damage of the interface.

d) Catastrophic fracture of the BGA assembly is predicted during the first temperature cycle with 60 % of the solder/IMC interface fractured. This is due to the relatively low input strength and toughness of the brittle-like interfaces.

ACKNOWLEDGEMENT

This research work is part of a collaborative research program under INTEL-UTM contract research project No. 4C015.

REFERENCES

[1] W. Zhong, Y. Chan, M. Alam, B. Wu, and J. Guan, "Effect of multiple reflow processes on the reliability of ball grid array (BGA) solder joints," *J. Alloys Compd.*, vol. 414, no. 1-2, pp. 123-130, 2006, doi: 10.1016/j.jallcom.2005.07.047.

[2] C.-H. Kuo, A. H. Hu, L. H. Hung, K.-T. Yang, and C.-H. Wu, "Life cycle impact assessment of semiconductor packaging technologies with emphasis on ball grid array," *J. Clean. Prod.*, vol. 276, no. 3, pp. 124301, 2020, doi: 10.1016/j.jclepro.2020.124301.

[3] J. H. Lau. "Flip Chip Technology versus FOWLP," in *Fan-Out Wafer-Level Packaging* 1st ed. Singapore: Springer, 2018, pp. 21-68.

[4] B. T. Ogunsemi, P. P. Ikubanni, A. A. Adediran, and O. O. Agboola, "Effect of stand-off height on the shear strength of ball grid array solder joints under varying pad sizes," *SN Appl. Sci.*, vol. 1, no. 1, pp. 36, 2019, doi: 10.1007/s42452-018-0044-5.

[5] E. H. Amalu, W. Lau, N. Ekere, R. Bhatti, S. Mallik, K. C. Otiaba, and G. Takyi, "A study of SnAgCu solder paste transfer efficiency and effects of optimal reflow profile on solder deposits," *Microelectron. Eng.*, vol. 88, no. 7, pp. 1610-1617, 2011, doi: 10.1016/j.mee.2011.02.104.

[6] J. Y. H. Chia, B. Cotterell, and T. C. Chai, "The mechanics of the solder ball shear test and the effect of shear rate," *Mater. Sci. Eng.: A*, vol. 417, no. 1-2, pp. 259-274, 2006, doi: 10.1016/j.msea.2005.10.064.

[7] D. S. Liu, C. Y. Kuo, C. L. Hsu, G. S. Shen, Y. R. Chen, and K. C. Lo, "Failure mode analysis of lead-free solder joints under high speed impact testing," *Mater. Sci. Eng.: A*, vol. 494, no. 1-2, pp. 196-202, 2008, doi: 10.1109/ICEPT.2008.4607136.

[8] P. Borgesen, L. Wentlent, T. Alghoul, R. Sivasubramony, M. Yadav, S. Thekkut, J. L. Then Cuevas, and C. Greene, "A mechanistic model of damage evolution in lead free solder joints under combinations of vibration and thermal cycling with varying amplitudes," *Microelectron. Reliab.*, vol. 95, pp. 65-73, 2019, doi: 10.1016/j.microrel.2019.02.001.

[9] M. A. A. Hanim, A. Ourdjini, I. S. R. Aisha, and O. S. Azlina, "Thermal cyclic test for Sn-4Ag-0.5Cu solders on high P Ni/Au and Ni/Pd/Au surface finishes," *J. Mech. Eng. Sci.*, vol. 9, pp. 1571, 2015, doi: 10.15282/jmes.9.2015.4.0152.

[10] C. L. Kao, and T. C. Chen, "Ball impact responses of Sn-1Ag-0.5 Cu solder joints at different temperatures and surface finishes," *Microelectron. Reliab.*, vol. 82, pp. 204-212, 2018, doi: 10.1016/j.microrel.2018.02.001.

[11] Z. Li, S. Belyakov, J. Xian, and C. Gourlay, "The influence of primary Cu_6Sn_5 size on the shear impact properties of Sn-Cu/Cu BGA joints," *J. Electron. Mater.*, vol. 47, no. 1, pp. 84-95, 2018, doi: 10.1007/s11664-017-5763-7.

[12] Y. Yao, and L. M. Keer, "Cohesive fracture mechanics based numerical analysis to BGA packaging and lead free solders under drop impact," *Microelectron. Reliab.*, vol. 53, no. 4, pp. 629-637, 2013, doi: 10.1016/j.microrel.2012.12.007.

[13] Directive 2002/95/EC of the European Parliament and of the Council of 27 January 2003 on the restriction of the use of certain hazardous substances in electrical and electronic equipment, Official Journal of the European Union, 13.2.2003, pp. L37/19-23. Retrieved from https://eur-lex.europa.eu/homepage.html

[14] H. Lee, C. Kim, C. Heo, C. Kim, J. H. Lee, and Y. Kim, "Effect of solder resist dissolution on the joint reliability of ENIG surface and Sn-Ag-Cu solder," *Microelectron. Reliab.*, vol. 87, pp. 75-80, 2018, doi: 10.1016/j.microrel.2018.05.017.

[15] A. Fahim, S. Ahmed, J. C. Suhling, and P. Lall, "Mechanical characterization of intermetallic compounds in SAC solder joints at elevated temperatures," in *2018 17th IEEE Intersociety Conf. Therm. Thermomech. Phenom. Electron. Syst. (ITherm)*, 2018, pp. 1081-1090, doi: 10.1109/ITHERM.2018.8419525.

[16] J. W. Yoon, S. W. Kim, and S. B. Jung, "IMC morphology, interfacial reaction and joint reliability of Pb-free Sn-Ag-Cu solder on electrolytic Ni BGA substrate," *J. Alloys Compd.*, vol. 392, no. 1-2, pp. 247-252, 2005, doi: 10.1016/j.jallcom.2004.09.045.

[17] T. An, F. Qin, and J. Li, "Mechanical behavior of solder joints under dynamic four-point impact bending," *Microelectron. Reliab.*, vol. 51, no. 5, pp. 1011-1019, 2011, doi: 10.1016/j.microrel.2010.12.009.

[18] X. Long, J. Xu, S. Wang, W. Tang, and C. Chang, "Understanding the impact response of lead-free solder at high strain rates," *Int. J. Mech. Sci.*, vol. 172, pp. 105416, 2020, doi: 10.1016/j.ijmecsci.2020.105416.

[19] J. Kim, H. Lee, and S. Jung, "Effect of surface treatment on the high-speed drop reliability of Pb-free solder interconnect," *Thin Solid Films*, vol. 547, pp. 120-124, 2013, doi: 10.1016/j.tsf.2013.04.056.

[20] D. Suh, D. W. Kim, P. Liu, H. Kim, J. A. Weninger, C. M. Kumar, et al., "Effects of Ag content on fracture resistance of Sn-Ag-Cu lead-free solders under high-strain rate conditions," *Mater. Sci. Eng. : A*, vol. 460-461, pp. 595-603, 2007, doi: 10.1016/j.msea.2007.01.145.

[21] A. Nourani, S. Akbari, and J. K. Spelt, "Fracture load prediction of BGA solder joints: Cohesive zone modeling and experimental verification," *Int. J. Solids Struct.*, vol. 90, pp. 30-44, 2016, doi: 10.1016/j.ijsolstr.2016.04.013.

[22] T. Henttonen, P. Mescher, D. Scott, H. Park, Y. Ko, and K. Engel, "Board level reliability study of next generation large die wafer level chip scale package structures," in *2018 Int. Wafer Level Packag. Conf. (IWLPC)*, 2018, pp. 1-9, doi: 10.23919/IWLPC.2018.8573297.

[23] T.-N. Tsai, "Thermal parameters optimization of a reflow soldering profile in printed circuit board assembly: A comparative study," *Appl. Soft Comput.*, vol. 12, no. 8, pp. 2601-2613, 2012, doi: 10.1016/j.asoc.2012.03.066.

[24] Y.-M. Jen, Y.-C. Chiou, and C.-L. Yu, "Fracture mechanics study on the intermetallic compound cracks for the solder joints of electronic packages," *Eng. Fail. Anal.*, vol. 18, no. 2, pp. 797-810, 2011, doi: 10.1016/j.engfailanal.2010.12.026.

[25] J. A. Depiver, S. Mallik, and E. H. Amalu, "Creep response of various solders used in soldering ball grid array (BGA) on printed circuit board (PCB),", pp. 1-9, 2019.
[26] Y. Zhang, C. Haibin, X. Ke, Y. Jinglei, and W. Jingshen, "The finite element model of the effect of the interface behavior of corner bond on the reliability of the BGA package under thermal cycling," in *2020 21st Int. Conf. Electron. Packag. Technol. (ICEPT)*, pp. 1-5, 2020, doi: 10.1109/ICEPT50128.2020.9202588.
[27] O. E. Pang, R. Daud, N. A. M. Amin, M. A. Rojan, and M. S. Abd Majid, "Finite element modeling of thin intermetallic compound layer fractures," *J. Mech. Eng. Sci.*, vol. 11, no. 1, pp. 2478, 2017, doi: 10.15282/jmes.11.1.2017.7.0228.
[28] L. Anand, "Constitutive equations for hot working of metals," *Int. J. Plast.*, vol. 1, pp. 213-231, 1985, doi: 10.1016/0749-6419(85)90004-X.
[29] J. Mi, Y.-F. Li, Y.-J. Yang, W. Peng, and H.-Z. Huang, "Thermal cycling life prediction of Sn-3.0Ag-0.5Cu solder joint using type-I censored data," *Scientific World J.*, vol. 2014, pp. 1-11, 2014, doi: 10.1155/2014/807693.
[30] A. Nourani, S. Akbari, G. Farrahi, and J. K. Spelt, "Strain-rate dependent influence of adherend stiffness on fracture load prediction of BGA solder joints," *Eng. Fract. Mech.*, vol. 186, pp. 119-133, 2017, doi: 10.1016/j.engfracmech.2017.09.027.
[31] E. Y. Seo, and J. E. Ryu, "Influence of reflow profile on thermal fatigue behaviors of solder ball joints," *J. Mater. Eng. Perform.*, vol. 29, no. 15, pp. 4095-4104, 2020, doi: 10.1007/s11665-020-04899-3.
[32] P. B. Thompson, R. Johnson, and S. P. Nadimpalli, "Effect of temperature on the fracture behavior of Cu/SAC305/Cu solder joints," *Eng. Fract. Mech.*, vol. 199, pp. 730-738, 2018, doi: 10.1016/j.engfracmech.2018.07.004.
[33] N. Shaffiar, Z. Lai, and M. N. Tamin, "Damage mechanics model for solder/intermetallics interface fracture process in solder joints," in *Key Eng. Mater.*, pp. 1409-1414, 2011, doi: 10.1109/EPTC.2008.4763533.
[34] A. Halouani, A. Cherouat, M. Miladi Chaabane, and M. Haddar, "Modeling and experimental investigation of damage initiation and propagation of LQFP package under thermal cycle," *Microsyst. Technol.*, vol. 26, pp. 3011-3021, 2020, doi: 10.1007/s00542-020-04884-9.
[35] L. Benabou, Z. Sun, and P.-R. Dahoo, "A thermo-mechanical cohesive zone model for solder joint lifetime prediction," *Int. J. Fatigue*, vol. 49, pp. 18-30, 2013, doi: 10.1016/j.ijfatigue.2012.12.008.
[36] D. Wang, and R. L. Panton, "Experimental study of void formation in eutectic and lead-free solder bumps of flip-chip assemblies," *Trans. J. Electron. Packag.*, vol. 128, pp. 202-207, 2006, doi: 10.1115/1.2229215.
[37] Z. B. Lai, N. Kamsah, W. K. Loh, and M. N. Tamin, "Mechanics of Sn-4Ag-0.5Cu solder joints in a ball grid array assembly during reflow and temperature cycles," in *Electron. Manuf. Technol. Symp. (IEMT), 2008 33rd IEEE/CPMT International*, pp. 1-8, 2008, doi: 10.1109/iemt.2008.5507864.
[38] JEDEC. Temperature Cycling. Virginia, 2009.
[39] M. N. Tamin, and N. M. Shaffiar. *Solder Joint Reliability Assessment. Finite Element Simulation Methodology*, Springer; 2014.
[40] W. Qiang, L. Lihua, C. Xuefan, W. Xiaohong, Y. Liu, S. Irving, T. Luk, "Experimental determination and modification of Anand model constants for Pb-free material 95.5Sn4.0Ag0.5Cu," in *Int. Conf. Therm. Mech. Multi-Physics Simul. Exp. Microelectron. Micro Syst. EuroSime 2007*, pp. 1-9, 2007, doi: 10.1109/ESIME.2007.359957.
[41] A. Schubert, R. Dudek, E. Auerswald, A. Gollhardt, B. Michel, and H. Reichl, "Fatigue life models for SnAgCu and SnPb solder joints evaluated by experiments and simulation," in *Electron. Compon. Technol. Conf.*, pp. 603-610, 2003, doi: 10.1109/ECTC.2003.1216343.
[42] X. Q. Shi, Z. P. Wang, W. Zhou, H. L. J. Pang, and Q. J. Yang, "A new creep constitutive model for eutectic solder alloy," *J. Electron. Packag.*, vol. 124, no. 2, pp. 85-90, 2002, doi: 10.1115/1.1462624.
[43] M. Amagai, "Chip scale package (CSP) solder joint reliability and modeling," *Microelectron. Reliab.*, vol. 39, no. 4, pp. 463-477, 1999, doi: 10.1016/S0026-2714(99)00017-7.
[44] B. A. Zahn, "Solder joint fatigue life model methodology for 63Sn37Pb and 95.5Sn4Ag0.5Cu materials," in *Electron. Compon. Technol. Conf. 2003 Proced. 53rd*, 2003, doi: 10.1109/ECTC.2003.1216261.
[45] M. N. Tamin, F. M. Nor, and W. K. Loh, "Hybrid experimental-computational approach for solder/IMC interface shear strength determination in solder joints," *IEEE Trans. Compon. Packag. Technol.*, vol. 33, no. 3, pp. 614-620, 2010, doi: 10.1109/TCAPT.2010.2050887.
[46] K. E. Yazzie, H. E. Fei, H. Jiang, and N. Chawla, "Rate-dependent behavior of Sn alloy–Cu couples: Effects of microstructure and composition on mechanical shock resistance," *Acta Mater.*, vol. 60, pp. 4336–4348, 2012, doi: 10.1016/j.actamat.2012.04.018.
[47] C. G. Dávila, and P. P. Camanho, "Decohesion elements using two and three-parameter mixed-mode criteria," in *Proc. Amer. Helicopter Soc. Conf.*, 2001.
[48] D. Mu, S. McDonald, J. Read, H. Huang, and K. Nogita, "Critical properties of Cu_6Sn_5 in electronic devices: Recent progress and a review," *Curr. Opin. Solid State Mater. Sci.*, vol. 20, no. 2, pp. 55-76, 2016, doi: 10.1016/j.cossms.2015.08.001.
[49] E. Dalton, G. Ren, J. Punch, and M. N. Collins, "Accelerated temperature cycling induced strain and failure behaviour for BGA assemblies of third generation high Ag content Pb-free solder alloys," *J. Mater. Des.*, vol. 154, pp. 184-191, 2018, doi: 10.1016/j.matdes.2018.05.030.
[50] T. Kobayashi, S. Terashima, and M. Tanaka, "Effect of thermomechanical fatigue on drop impact properties of Sn-Ag-Cu lead-free solder joints," in *2012 IEEE 14th Electron. Packag. Technol. Conf. (EPTC)*, pp. 215-218, 2012, doi: 10.1109/EPTC.2012.6507081.
[51] T. An, C. Fang, F. Qin, H. Li, T. Tang, and P. Chen, "Failure study of Sn37Pb PBGA solder joints using temperature cycling, random vibration and combined temperature cycling and random vibration tests," *Microelectron. Reliab.*, vol. 91, pp. 213-226, 2018, doi: 10.1016/j.microrel.2018.10.003.